State of charge estimation for lithium-ion battery based on an Intelligent Adaptive Extended Kalman Filter with improved noise estimator

Sun, D., Yu, X., Wang, C., Zhang, C., Huang, R., Zhou, Q., Amietszajew, T. & Bhagat, R.

DOI 10.1016/j.energy.2020.119025
ISSN 0360-5442

Publisher: Elsevier

State of Charge Estimation for Lithium-Ion Battery based on an Intelligent Adaptive Extended Kalman Filter with improved noise estimator

Daoming Sun[a], Xiaoli Yu[a]*, Chongming Wang[b], Cheng Zhang[b], Rui Huang[a],

Quan Zhou[c], Taz Amietszajew[b], Rohit Bhagat[b]

[a] *Department of Energy Engineering, Zhejiang University, Hangzhou 310027, China*

[b] *Centre for Advanced Low Carbon Propulsion Systems, Coventry University, Coventry, United Kingdom, CV1 5FB*

[c] *Department of Mechanical Engineering, The University of Birmingham, Birmingham B15 2TT, United Kingdom*

* Corresponding author *E-mail address:* yuxl@zju.edu.cn; (Prof X. Yu)

Abstract: Adaptive extended Kalman filter (AEKF) is widely used for lithium-ion battery (LIBs) state of charge (SOC) estimation. Innovation covariance matrix (ICM) of AEKF is estimated by fixed-length error innovation sequence (EIS) (the difference between measured and estimated voltages), which doesn't consider the distribution change of EIS. However, the distribution of EIS will change due to load current dynamics or error of battery model. Failing to consider the distribution change of EIS will lead to SOC estimation inaccuracy. To address this problem, this paper proposed an intelligent adaptive extended Kalman filter (IAEKF) method that can detect the moment of distribution change of EIS by the maximum likelihood function. Then, the ICM is updated based on the EIS after that moment to improve the SOC estimation accuracy. Results show that the proposed IAEKF method improves SOC estimation accuracy. Compared to that of the AEKF, the Root Mean Squared Error (RMSE) and the Mean Absolute Error (MAE) of SOC based on IAEKF decrease significantly by 43.34% and 55.80%, respectively, while the computation time only increases by 4.59%. In the end, the effect of initial parameters on the SOC estimation accuracy was analysed. It is found that the proposed IAEKF method is robust against parameter uncertainties.

Keywords: Lithium-ion battery; State of Charge; Innovation covariance matrix; Distribution change; Intelligent adaptive extended Kalman filter;

Abbreviation

ACKF: Adaptive cubature Kalman filter
AEKF: Adaptive EKF
APF: Adaptive PF
AUKF: Adaptive UKF
CKF: Cubature Kalman filter
DEKF: Dual EKF
DUKF: Dual UKF
ECM: Equivalent circuit model
EIS: Error innovation sequence
EKF: Extended Kalman filter
EM: Electrochemical mode
EMS: Energy Management Strategy
FS: Fuzzy System
GA: Genetic Algorithm
IAEKF: Intelligent AEKF
ICM: Innovation covariance matrix
LIBs: Lithium-ion batteries
LSTM: Long Short-Term Memory
MAE: Mean absolute error
ML: Maximum likelihood
NN: Neural Network
OCV: Open circuit voltage
PDF: Probability density function
PF: Particle filter
PSO: Particle swarm optimization
RLS: Recursive least square
RMSE: Root mean squared error
SA: Simulated Annealing
SOC: State of Charge
STD: Standard deviation
SVM: Support Vector Machine
UKF: Unscented Kalman filter

1. Introduction

The energy crisis and environment pollution are the primary force that drive the fast development of renewable energy [1]. Renewable energy, such as solar and wind generation, are becoming increasing popular for power generation [2]. The clean power energy generated from the solar and wind energy are gradually changing the energy supply structure in many kinds of industries, such as residential electricity, automobile industry and aerospace industry. However, renewable energy is facing some difficulties in mass promotion due to the intermittent and fluctuating features caused by weather resources [3]. Therefore, it is urgent to develop highly efficient distributive energy storage devices. Due to the advantages of high energy density, long lifespan, high efficiency and low self-discharge rate [4], Lithium-ion batteries (LIBs) are widely used for energy storage and supply in various applications, especially for electric vehicles. The state of charge (SOC) is one of the key state indicators that must be estimated for normal operation of LIBs. On the one hand, inaccurate SOC estimation may lead to the risk of over-discharge or over-charge of LIBs, which will accelerate ageing and shorten the lifetime of the LIBs [5]. On the other hand, inaccurate SOC estimation will affect the energy management strategy (EMS) for electric vehicle [6]. Therefore, improving the accuracy of SOC estimation is of high importance to both battery safety operation and performance optimisation.

1.1 Literature Review of SOC estimation method

The existing SOC estimation methods fall into four categories: 1) coulomb counting method [7, 8]; 2) open-circuit voltage (OCV) method [9, 10]; 3) data-driven method [11]; 4) model-based method [12, 13].

The coulomb counting method, which integrates the current over time, is easy to implement. However, prior information about initial SOC must be provided. Further, as an open-loop method, it is vulnerable to accumulated error over time [14].

The OCV method is based on the terminal voltage measured at the equilibrium state of LIB, which takes a long time to reach due to the slow internal diffusion dynamics of LIBs [15].

The data-driven methods, such as neural networks (NN) [16], support vector regression (SVM) [17] and fuzzy system (FS) [18, 19], are intelligent methods with self-learning function. Compared to SVM and FS, NN is often adopted and designed to estimate the SOC of LIBs due to its strong nonlinear modelling ability. The NN can be further classified into three categories, such as ordinary-NN [20], deep-NN [21] and long short-term memory-NN (LSTM-NN) [22, 23]. Compared with ordinary-NN, deep-NN has better generalization ability for SOC estimation [21]. Compared with ordinary-NN and deep-NN, LSTM-NN can not only capture the short-term correlation between data, but also the long-term correlation between data [24]. The data-driven methods can estimate the SOC without detailed knowledge of battery electrochemical dynamics. However, these data-driven methods also have some disadvantages. Firstly, it is difficult to design the structure of deep-NN so that they can have better generalization ability. Second, the data-driven methods need substantial data to train and validate model. Last but not least, it is difficult to optimize the parameters of deep-NN and LSTM-NN due to the complex structure of such NNs.

The model-based methods can be further classified into state observer methods [25] and filter-based methods [26] based on the adopted principle. The state observer methods are designed to observe the state of the system based on control theory. The commonly used state observer methods include proportional-integral observer [27], $H\infty$ observer [28, 29], sliding mode observer and nonlinear observer [30, 31]. The state observer methods can cope well with the model uncertainty and external disturbance. However, it is difficult to design the state observer and the proof of convergence performance is complex. The filter-based methods estimate the state of the system from the perspective of eliminating noise. The filter-based methods, which combine the battery model with a closed-loop SOC estimation iteration process, have proved to be accurate and implementable in

real-time due to low complexity. Compared with state observer methods, filter-based methods have lower computation complexity, and it is easy to be implemented for online SOC estimation. In addition, the filter-based methods avoid the complex proof process of convergence performance compared with state observer methods.

In comparison with the coulomb counting method and OCV method, the model-based methods have better robustness because of the closed-loop correction process [32]. Compared with data-driven methods, the model-based methods do not require extensive data to train the model and the computational complexity is lower [33]. Comparing two kinds of model-based methods – state observer methods and filter-based methods mentioned above, the filter-based methods are more suitable for online SOC estimation of LIBs. Therefore, the filter-based methods become the popular online SOC estimation methods of LIBs.

The filter-based methods have been widely used for SOC estimation of LIBs [34]. They usually consist of three parts: 1) battery model; 3) parameter identification algorithm; and 3) filter algorithm. There are two main kinds of battery models – electrochemical model (EM) [35, 36] and equivalent circuit model (ECM) [37]. The ECMs are widely used for online state estimation due to a good balance between accuracy and computational complexity [38]. Among the ECMs, Thevenin model is often adopted for online SOC estimation considering both accuracy of model and difficulties of parameter identification. Thevenin model consists of an OCV, an internal resistor and a RC networks. Many types of functions, such as polynomial function, logarithmic function and exponential function, have been proposed for OCV modelling [39]. Among these types of functions, polynomial function is widely used for OCV model due to low computation complexity and good flexibility by adjusting the order of polynomial. Once the OCV model is obtained, the other parameters in the ECM can be estimated from experimental data for the following state estimation. Optimization algorithms, such as genetic algorithm (GA) [40, 41], particle swarm optimization (PSO) algorithm [42] and simulated

annealing (SA) algorithm [43], have been used for offline parameter estimation in the ECM. As the parameters in the ECM are time-varying in the operation condition, many kinds of recursive least square (RLS) methods were proposed for online parameter identification [44, 45]. With the parameters obtained from RLS methods online, the SOC of LIBs can be estimated using a variety of state estimation algorithms, such as extended Kalman filter (EKF) [46, 47], unscented Kalman filter (UKF) [48], cubature Kalman filter (CKF) [49], and particle filter (PF) [50]. However, the measurement and process noise covariance are assumed to be constant in these state filters.

However, the noise covariance may change in the actual operation condition. To improve the SOC estimation accuracy, the adaptive filters, such as adaptive EKF (AEKF) [51], adaptive UKF (AUKF) [52, 53], adaptive CKF (ACKF) [54, 55] and adaptive PF (APF) [56] that can adjust the noise covariance in real-time, are proposed for state estimation.

Recently, dual-filters were proposed for simultaneous parameter and state estimation, such as dual EKF (DEKF) [57] and dual UKF (DUKF) [58]. The first filter is used for parameter identification, while the second one is used for SOC estimation. Compared with filters based on ECM with offline-identified parameters, the dual filters can achieve better SOC accuracy. In view of the different change rate of the parameters and state, multi-time scale dual filter, such as multi-time scale DEKF [59], is proposed for simultaneous parameter and state estimation. Compared with the estimation accuracy of dual filters, multi-time scale dual filters can achieve similar estimation accuracy with much less computational complexity. To update the noise covariance online, double adaptive filters, such as multi-time scale dual AEKF [60] and multi-time scale dual adaptive PF [61], are proposed for parameter and state estimation. Compared to multi-time scale dual filters, the multi-time scale dual adaptive one improves the SOC estimation accuracy with the online-updated measurement noise covariance.

In spite of these improvement, these filters didn't consider the distribution change of the EIS, which leads to inaccurate estimation of ICM. In the existing AEKF method, the ICM is updated based on fixed-length EIS. This method, therefore, can't detect change of the ICM. However, the distribution of EIS can change under dynamic load profiles because the measurement error of the current/voltage sensors depends on the signal amplitude. Further, the modelling and state estimation error also contribute to the distribution change of the EIS. Before and after the moment of distribution change of EIS, the ICM are different. Therefore, a fixed-length EIS will lead to inaccurate estimation of ICM, which will affect the SOC estimation accuracy negatively.

1.2 Contribution of the paper

In order to improve the accuracy of SOC, an Intelligent Adaptive Extended Kalman Filter (IAEKF) is proposed for SOC estimation. A detection window of the EIS is set, and the moment of distribution change of EIS is then detected by the maximum likelihood function. The EIS after that moment is selected to estimate the ICM. With the improved ICM estimation value, the noise covariance can be estimated accurately. By updating the noise covariance online, the SOC estimation accuracy of LIBs can be improved significantly.

1.3 Organization of the paper

The outline of the paper is as follows: The battery model is presented in Section 2. Section 3 presents the online estimation of the ECM parameters using forgetting factor-RLS (FF-RLS). The initial parameters are obtained by GA. In Section 4, the IAEKF method is proposed to improve the SOC estimation accuracy, followed by the verification of the effectiveness and robustness of the algorithm. In the end, conclusions are given.

2. Battery model

The ECMs are widely used to describe the internal dynamics and estimate SOC of LIBs. Considering the model complexity, accuracy, and robustness, Thevenin model is chosen for the SOC estimation, as shown in Fig. 1. This ECM model consists of a voltage source U_{oc}, a series-connected ohmic resistor R_s, and an RC network (parallel-connected diffusion resistance R_p and diffusion capacitance C_p).

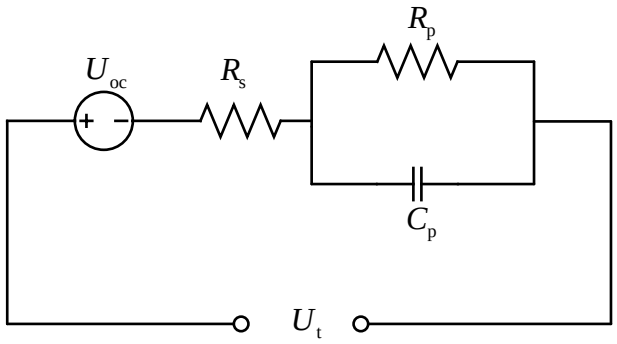

Fig. 1. Schematic diagram of the Thevenin model

SOC is defined as the ratio of remaining capacity and the nominal capacity. The relationship of SOC at a different time can be described as Eq. (1):

$$\mathrm{SOC}(t) = \mathrm{SOC}(t_0) - \int_{t_0}^{t} \frac{\eta \cdot i dt}{3600 \cdot \mathrm{C_n}} \tag{1}$$

where $\mathrm{SOC}(t)$ and $\mathrm{SOC}(t_0)$ are the SOC at the time t and initial time t_0, respectively. η is the charge and discharge efficiency of the battery. i is the electric current with a positive value during discharge and a negative value during charge. $\mathrm{C_n}$ represents the nominal capacity of the battery.

The dynamic electrical behaviours of the battery can be described by the following equation,

$$\begin{cases} \dot{U_p} = \dfrac{i}{C_p} - \dfrac{U_p}{C_p \cdot R_p} \\ U_t = U_{oc} - U_p - i \cdot R_0 \end{cases} \tag{2}$$

where $\dot{U}_{\mathrm{p}}$ is the derivative of polarization voltage U_{p}. U_{t} is the terminal voltage and U_{oc} represents the OCV.

Discretising Eq. (1) and Eq. (2), the state-space model of a LIB can be written as:

$$\text{State equation:} \quad \begin{cases} U_{\mathrm{p},k} = \exp\left(-\dfrac{\Delta t}{C_{\mathrm{p},k-1}R_{\mathrm{p},k-1}}\right)\cdot U_{\mathrm{p},k-1} + \left(1-\exp\left(-\dfrac{\Delta t}{C_{\mathrm{p},k-1}R_{\mathrm{p},k-1}}\right)\right)\cdot R_{\mathrm{p},k-1} i_{k-1} \\ \mathrm{SOC}_k = \mathrm{SOC}_{k-1} - \dfrac{\eta_i \cdot i_{k-1}\cdot \Delta t}{3600\cdot \mathrm{C_n}} \end{cases} \tag{3}$$

$$\text{Measurement equation:} \quad U_{\mathrm{t},k} = U_{\mathrm{oc},k} - U_{\mathrm{p},k} - i_k \cdot R_{0,k} \tag{4}$$

where $U_{\mathrm{p},k}$, $U_{\mathrm{oc},k}$ and $U_{\mathrm{t},k}$ represent the polarization voltage, OCV and terminal voltage at the time step k, respectively. The OCV is expressed as $U_{\mathrm{oc}}(\mathrm{SOC}) = K_0 + K_1\cdot\mathrm{SOC} + K_2\cdot\mathrm{SOC}^2 + \ldots + K_n\cdot\mathrm{SOC}^n$. Eq. (3) and (4) can be described as Eq. (5)

$$\begin{cases} \mathbf{x}_k = \mathbf{A}_{k-1}\mathbf{x}_{k-1} + \mathbf{B}_{k-1}\mathbf{u}_{k-1} + \boldsymbol{\omega}_k \\ \mathbf{y}_k = g(\mathbf{x}_k, \mathbf{u}_k) + \boldsymbol{\upsilon}_k \end{cases} \tag{5}$$

where $\mathbf{x}_k = \begin{bmatrix} U_{\mathrm{p},k} \\ \mathrm{SOC}_k \end{bmatrix}$, $\mathbf{A}_{k-1} = \begin{bmatrix} \exp\left(-\dfrac{\Delta t}{C_{\mathrm{p},k-1}R_{\mathrm{p},k-1}}\right) & 0 \\ 0 & 1 \end{bmatrix}$, $\mathbf{B}_{k-1} = \begin{bmatrix} \left(1-\exp\left(-\dfrac{\Delta t}{C_{\mathrm{p},k-1}R_{\mathrm{p},k-1}}\right)\right)\cdot R_{\mathrm{p},k-1} \\ \dfrac{\eta_i \Delta t}{3600\cdot \mathrm{C_n}} \end{bmatrix}$, $\mathbf{u}_k = i_k$,

$\mathbf{y}_k = U_{\mathrm{t},k}$, $g(\mathbf{x}_k, \mathbf{u}_k) = U_{\mathrm{oc},k} - U_{\mathrm{p},k} - i_k \cdot R_{\mathrm{s},k}$. $\boldsymbol{\omega}_k$ and $\boldsymbol{\upsilon}_k$ are the process noise and measurement noise, respectively.

3. Parameter identification for ECM

The parameters ($K_0, K_1, K_2, \ldots, K_n$) of the OCV model are estimated by fitting ($\mathrm{SOC}, \mathrm{OCV}$) measured from the OCV tests. Then initial parameters ($R_{\mathrm{s}}, R_{\mathrm{p}}, C_{\mathrm{p}}$) of the ECM are estimated based on GA by minimizing the sum of squared terminal voltage error, as shown in Eq. (6)

$$\min\ f(R_{\mathrm{s}}, R_{\mathrm{p}}, C_{\mathrm{p}}) = \sum_{k=1}^{N_1}\left(U_{\mathrm{t},k}(t) - U_{\mathrm{t},k}^{*}(t)\right)^2 \tag{6}$$

where $U_{\mathrm{t},k}^{*}(t)$ is the measured terminal voltage, N_1 is the length of pulse discharge sequence.

Considering that the parameters of the ECM change under the actual operation condition, the parameters (R_s, R_p, C_p) of the ECM are updated online. In view of both complexity and accuracy, forgetting factor-RLS (FF-RLS) is used for online parameter identification with the initial parameters obtained above. The detailed implementation process of FF-RLS algorithm can be found in Ref. [62].

4. IAEKF for SOC estimation

4.1 AEKF algorithm

The AEKF is a combination of EKF and adaptive law. The EKF consists of two parts: model prediction step and state correction step. In the prediction step, the states at step k are predicted based on the states at step $k-1$. In the correction step, the predicted states are corrected using the new measurements at the time step k. EKF has been widely used for state estimation of nonlinear systems. The adaptive law of the AEKF is to update the noise covariance online. In general, the state and measurement equations used in the EKF are expressed as follows:

$$\begin{cases} \mathbf{x}_k = f\left(\mathbf{x}_{k-1}, \mathbf{u}_{k-1}\right) + \boldsymbol{\omega}_k \\ \mathbf{y}_k = g\left(\mathbf{x}_k, \mathbf{u}_k\right) + \boldsymbol{\upsilon}_k \end{cases} \tag{7}$$

where $\mathbf{x}_k$ is the system state vector, $\mathbf{y}_k$ is the measurement vector, $\mathbf{u}_k$ is the known input vector, $\boldsymbol{\omega}_k$ is the Gaussian process noise, $\boldsymbol{\upsilon}_k$ is the Gaussian measurement noise, $f(\mathbf{x}_k, \mathbf{u}_k)$ is a nonlinear state function, and $g(\mathbf{x}_k, \mathbf{u}_k)$ is a nonlinear measurement function.

The detailed algorithm of AEKF [28] is as follows:

Model prediction step

(1) Initialization

$$\hat{\mathbf{x}}_0^+ = E\left[\mathbf{x}_0\right], \quad P_0^+ = E\left[\left(\mathbf{x}_0 - \hat{\mathbf{x}}_0^+\right)\left(\mathbf{x}_0 - \hat{\mathbf{x}}_0^+\right)^T\right] \tag{8}$$

(2) State estimation

$$\hat{\mathbf{x}}_k^- = \mathbf{A}_{k-1}\hat{\mathbf{x}}_{k-1} + \mathbf{B}_{k-1}\mathbf{u}_{k-1} \tag{9}$$

(3) Error covariance time update

$$\mathbf{P}_{xx,k|k-1} = \mathbf{A}_k\mathbf{P}_{xx,k-1|k-1}\mathbf{A}_k^{\mathrm{T}} + \mathbf{Q}_{k\text{-}1} \tag{10}$$

State correction step

(4) Kalman gain matrix

$$\mathbf{K}_k = \mathbf{P}_{xx,k|k-1}\mathbf{C}_k^{\mathrm{T}}\left(\mathbf{C}_k\mathbf{P}_{xx,k|k-1}\mathbf{C}_k^{\mathrm{T}} + \mathbf{R}_k\right)^{-1} \tag{11}$$

(5) Error innovation calculation

$$\mathbf{e}_k = \mathbf{y}_k - g\left(\hat{\mathbf{x}}_k^-, \mathbf{u}_k\right) \tag{12}$$

(6) State estimate update

$$\hat{\mathbf{x}}_k^+ = \hat{\mathbf{x}}_k^- + \mathbf{K}_k\mathbf{e}_k \tag{13}$$

(7) Error covariance update

$$\mathbf{P}_{xx,k|k} = \left(\mathbf{I} - \mathbf{K}_k\mathbf{C}_k\right)\mathbf{P}_{xx,k|k-1} \tag{14}$$

(8) Adaptive law-covariance matching

$$\mathbf{H}_k = \frac{1}{M}\sum_{i=k-M+1}^{k}\mathbf{e}_k\mathbf{e}_k^T \tag{15}$$

$$\mathbf{R}_k = \mathbf{H}_k + \mathbf{C}_k\mathbf{P}_{xx,k|k}\mathbf{C}_k^T \tag{16}$$

$$\mathbf{Q}_k = \mathbf{K}_k\mathbf{H}_k\mathbf{K}_k^{\mathrm{T}} \tag{17}$$

where $\mathbf{A}_{k-1}=\left.\frac{\partial f\left(\mathbf{x}_{k-1},\mathbf{u}_{k-1}\right)}{\partial x}\right|_{\mathbf{x}=\hat{\mathbf{x}}_{k-1}^{-}}$, $\mathbf{C}_{k-1}=\left.\frac{\partial g\left(\mathbf{x}_{k-1},\mathbf{u}_{k-1}\right)}{\partial x}\right|_{\mathbf{x}=\hat{\mathbf{x}}_{k-1}^{-}}$.

The ICM $\mathbf{H}_k$ is online updated based on Eq. (11). Then the noise covariance $\mathbf{R}_k$ and $\mathbf{Q}_k$ are updated based on Eq. (12) and (13) in the AEKF algorithm. When the AEKF algorithm is applied for SOC estimation, the coefficient matrix $\mathbf{A}_{k-1}$, $\mathbf{B}_{k-1}$ and $\mathbf{C}_{k-1}$ can be found in Section 2.1.

4.2 Intelligent noise estimator

4.2.1 Detection of the change of the distribution of the EIS

In the AEKF algorithm, the ICM is estimated based on the fixed length (M) EIS, as shown in Eq. (15). However, the distribution of EIS changes because the measurement error of the current/voltage sensors depends on the signal amplitude. Further, the modelling and state estimation error also contribute to the distribution change of the EIS. Therefore, for the estimation of ICM, it is better to detect the moment of change of the statistic distribution of the EIS. To solve this problem, an intelligent approach is proposed for estimating ICM through the detection of the distribution change of the EIS.

In order to detect the change of this distribution, a detection window with length $2N$ is considered. The EIS inside this window is expressed as $[e_{k-2N}, e_{k-2N+1}, \ldots, e_{k-1}]$, where e_k is the EIS at the time step k in Eq. (12). Assuming a white Gaussian noise distribution, the EIS within this detection window has zero mean and variance σ^2. Therefore, the probability density function (PDF) of the EIS inside the detection window can be expressed as follows:

$$f\left(e_k\right)=\frac{1}{\sqrt{2\pi\sigma^2}}e^{-\frac{e_k^2}{2\sigma^2}}, e_k \sim N\left(0,\sigma^2\right) \tag{18}$$

If the distribution of the EIS changes slowly, the noise statistics within the detection window with the newly added EIS will remain nearly constants. In this case, the measurement noise PDF in the detection window will be almost fixed. Therefore, the ICM $\mathbf{H}_k$ can be computed with acceptable

approximation from Eq. (15). Otherwise, if the distribution of the EIS changes rapidly, two different PDFs may occur in the detection window. Then Eq. (15) cannot yield an accurate estimation of the ICM. Therefore, it is required to detect the moment of distribution change inside the detection window. Once the moment of distribution change of EIS is detected, the data received before that moment cannot be used to assess the ICM after the moment, and the estimation window length must be reset. On the other hand, if there is no distribution change of EIS, more data points can generate a better covariance estimation. Therefore, an increase of window length between two moments of distribution change leads to the improvement of estimation accuracy of the ICM. Therefore, in the proposed algorithm, estimation window length increases between two moments of distribution change and is reset once the new moment of distribution change arrives.

In this paper, the moment of distribution change of EIS is detected based on the square of the EIS. Let $W_k = e_k^2$, then cumulative distribution function of the square of the EIS W_k can be obtained as the following equation, where W_k is square of the EIS at the time k.

$$F_{W_k}(w_k) = P\left(-\sqrt{w_k} \le e_k \le \sqrt{w_k}\right) = F\left(\sqrt{w_k}\right) - F\left(-\sqrt{w_k}\right) \tag{19}$$

The PDF of W_k can be obtained by differentiating both sides of Eq. (19) as follows:

$$f_{W_k}(w_k) = \frac{1}{2\sqrt{w_k}}\left(f\left(\sqrt{w_k}\right) + f\left(-\sqrt{w_k}\right)\right) = \frac{1}{\sqrt{2\pi\sigma^2 w_k}} e^{-\frac{w_k}{2\sigma^2}} \tag{20}$$

The variance of measurement noise inside the detection window of length $2N$ can be estimated based on the Maximum-Likelihood (ML) method. If sequence W inside the detection window is given as $W = [W_{k-2N}, \ldots, W_{k-N}, \ldots, W_{k-1}]$, since data of sequence W are independent, the PDF of the sequence W equals the product of the individual sequence data.

$$f_W(w) = \prod_{n=k-2N}^{k-1} \frac{1}{\sqrt{2\pi\sigma^2 w_n}} e^{-\frac{w_n}{2\sigma^2}} \tag{21}$$

where $W=[w_{k-2N},\ldots,w_{k-N},\ldots,w_{k-1}]$. In order to obtain the variance σ^2 based on ML estimation $\ln(f_W(w))$ must be maximised. From Eq. (21), we can get

$$\ln(f_W(w))=-\frac{1}{2}\sum_{n=k-2N}^{k-1}\left[\ln(2\pi\sigma^2 w_n)+\frac{w_n}{\sigma^2}\right] \tag{22}$$

Let $\frac{\partial\ln(f_W(w))}{\partial\sigma^2}=0$, then σ^2 can be obtained as follows

$$\sigma^2=\frac{1}{2N}\sum_{n=k-2N}^{k-1}w_n \tag{23}$$

Substitute Eq. (23) into Eq. (22), we can obtain the logarithmic ML function value F_1, as shown in Eq. (24)

$$\begin{aligned}F_1&=\max\left(\ln(f_W(w))\right)\\&=-\frac{1}{2}\sum_{n=k-2N}^{k-1}\left[\ln(2\pi\sigma^2 w_n)+\frac{w_n}{\sigma^2}\right]\end{aligned} \tag{24}$$

In order to detect the moment of distribution change, the middle point of the sliding detection window must be checked at each time step. If the point checked is just the moment of distribution change, the PDF in the whole of the detection window equals the product of the PDFs in two regions:

$$f_W(w)=\prod_{n=k-N}^{k-1}\frac{1}{\sqrt{2\pi\sigma_1^2 w_n}}e^{-\frac{w_n}{2\sigma_1^2}}\prod_{n=k-2N}^{k-N-1}\frac{1}{\sqrt{2\pi\sigma_2^2 w_n}}e^{-\frac{w_n}{2\sigma_2^2}} \tag{25}$$

where the sequences in the first and second half of the detection window follow Gaussian distribution with variance σ_1^2 and σ_2^2, respectively. From Eq. (25)

$$\ln(f_W(w))=-\frac{1}{2}\sum_{n=k-N}^{k-1}\left[\ln(2\pi\sigma_1^2 w_n)+\frac{w_n}{\sigma_1^2}\right]-\frac{1}{2}\sum_{n=k-2N}^{k-N-1}\left[\ln(2\pi\sigma_2^2 w_n)+\frac{w_n}{\sigma_2^2}\right] \tag{26}$$

Let $\frac{\partial\ln(f_W(w))}{\partial\sigma_1^2}=0$ and $\frac{\partial\ln(f_W(w))}{\partial\sigma_2^2}=0$, σ_1^2 and σ_2^2 can be obtained as follows:

$$\sigma_1^2=\frac{1}{N}\sum_{n=k-N}^{k-1}w_n \tag{27}$$

$$\sigma_2^2 = \frac{1}{N}\sum_{n=k-2N}^{k-N-1} w_n \tag{28}$$

Substitute Eq. (27) and Eq. (28) into Eq. (26), we can obtain the logarithmic ML function value F_2 under the conditions of distribution change, as shown in Eq. (29):

$$\begin{aligned} F_2 &= \max\left(f_W(w)\right) \\ &= -\frac{1}{2}\sum_{n=k-N}^{k-1}\left[\ln\left(2\pi\sigma_1^2 w_n\right)+\frac{w_n}{\sigma_1^2}\right]-\frac{1}{2}\sum_{n=k-2N}^{k-N-1}\left[\ln\left(2\pi\sigma_2^2 w_n\right)+\frac{w_n}{\sigma_2^2}\right] \end{aligned} \tag{29}$$

By comparing F_1 and F_2, it can be determined whether there is a distribution change of EIS within the detection window. If the moment of distribution change of EIS lies inside the detection window, the value F_2 will be greater than F_1; otherwise, the opposite is true. Therefore, the moment of distribution change of EIS can be detected based on the condition relation as Eq. (30), where Th is a threshold value that can be set according to trial and error.

$$F_2 - F_1 > Th \tag{30}$$

The chance of detection of moment of distribution change of EIS becomes smaller as Th increases. Conversely, if Th is too small, even slight variations in the distribution can cause a false alarm. Based on the simulation and test, it is found that $Th = N$ is a proper choice. Next, the condition expressed in Eq. (30) must be checked at each time step. If this condition is met, distribution change is detected, and the data received prior to detected moment can't be used for estimating the ICM afterwards. An initial window length $L_{\text{ini}} = 2$ is set. If no distribution change of EIS is detected, estimation window length will be increased. As the computation load increases with the increase of window length, a maximum value $L_{\max}$ should be set for the window length. Therefore, adaptive tuning of window length is described as follows

$$\begin{cases} L_k = 2, \text{if } \left(F_2 - F_1\right) > Th \\ L_k = L_{k-1} + 1, \text{if } \left(F_2 - F_1\right) \le Th \,\&\, L_k \le L_{\max} \\ L_k = L_{\max}, \text{if } L_k > L_{\max} \end{cases} \tag{31}$$

In order to reduce computational complexity, Eq. (24) and (29) are simplified as follows:

$$F_1 = -\frac{1}{2}\left[2N\ln(2\pi) + 2N\ln(\sigma^2) + \sum_{n=k-2N}^{k-1} \ln(w_n) + 2N \right] \tag{32}$$

$$\begin{aligned} F_2 = &-\frac{1}{2}\left[N\ln(2\pi) + N\ln(\sigma_1^2) + \sum_{n=k-N}^{k-1} \ln(w_n) + N \right] \\ &-\frac{1}{2}\left[N\ln(2\pi) + N\ln(\sigma_2^2) + \sum_{n=k-2N}^{k-N-1} \ln(w_n) + N \right] \end{aligned} \tag{33}$$

Thus, $F_2 - F_1$ can be simplified as follows

$$F_2 - F_1 = N \cdot \ln\left(\frac{\sigma^2}{\sigma_1 \sigma_2} \right) \tag{34}$$

Three parameters (σ, σ_1 and σ_2) in Eq. (34) can be determined based on Eq. (23), Eq.(27) and Eq.(28) respectively. As such, calculation of Eq. (34) is relatively simple and easy to implement.

4.2.2 Noise estimator based on the selected innovation sequence

Based on the detection method of distribution change, the EIS after that moment can be selected for the estimation of the ICM. The ICM $\mathbf{H}_k$ in Eq. (15) can be estimated as follows:

$$\mathbf{H}_k = \frac{1}{L_k} \sum_{i=k-L_k+1}^{k} \mathbf{e}_k \mathbf{e}_k^{\mathrm{T}} \tag{35}$$

where L_k is dynamically updated based on Eq. (31).

With the obtained ICM, the covariance of measurement and process noise can be estimated as follows:

$$\begin{cases} \mathbf{R}_k = \mathbf{H}_k + \mathbf{C}_k \mathbf{P}_k \mathbf{C}_k^{\mathrm{T}} \\ \mathbf{Q}_k = \mathbf{K}_k \mathbf{H}_k \mathbf{K}_k^{\mathrm{T}} \end{cases} \tag{36}$$

In the comparison of the total computation load of AEKF algorithm, the computation load of the added part for the detection of distribution change is negligible.

4.3 Framework of IAEKF algorithm

Fig. 2 shows a flow chart of the IAEKF-based SOC estimation. The window length of the EIS is no longer fixed but dynamically tuned based on the detection of the moment of distribution change of EIS, as shown in the blue part of Fig. 2. With the selected EIS, the ICM $\mathbf{H}_k$ is updated based on Eq. (35), as shown in the yellow part of Fig. 2. Following the estimation of ICM $\mathbf{H}_k$, then the covariance of measurement noise ($\mathbf{R}_k$) and process noise ($\mathbf{Q}_k$) are estimated based on Eq. (36). The number N_t in Fig. 2 represents the total length of the time sequence in the random charge and discharge test. $k > N_t$ represents the end of SOC estimation process.

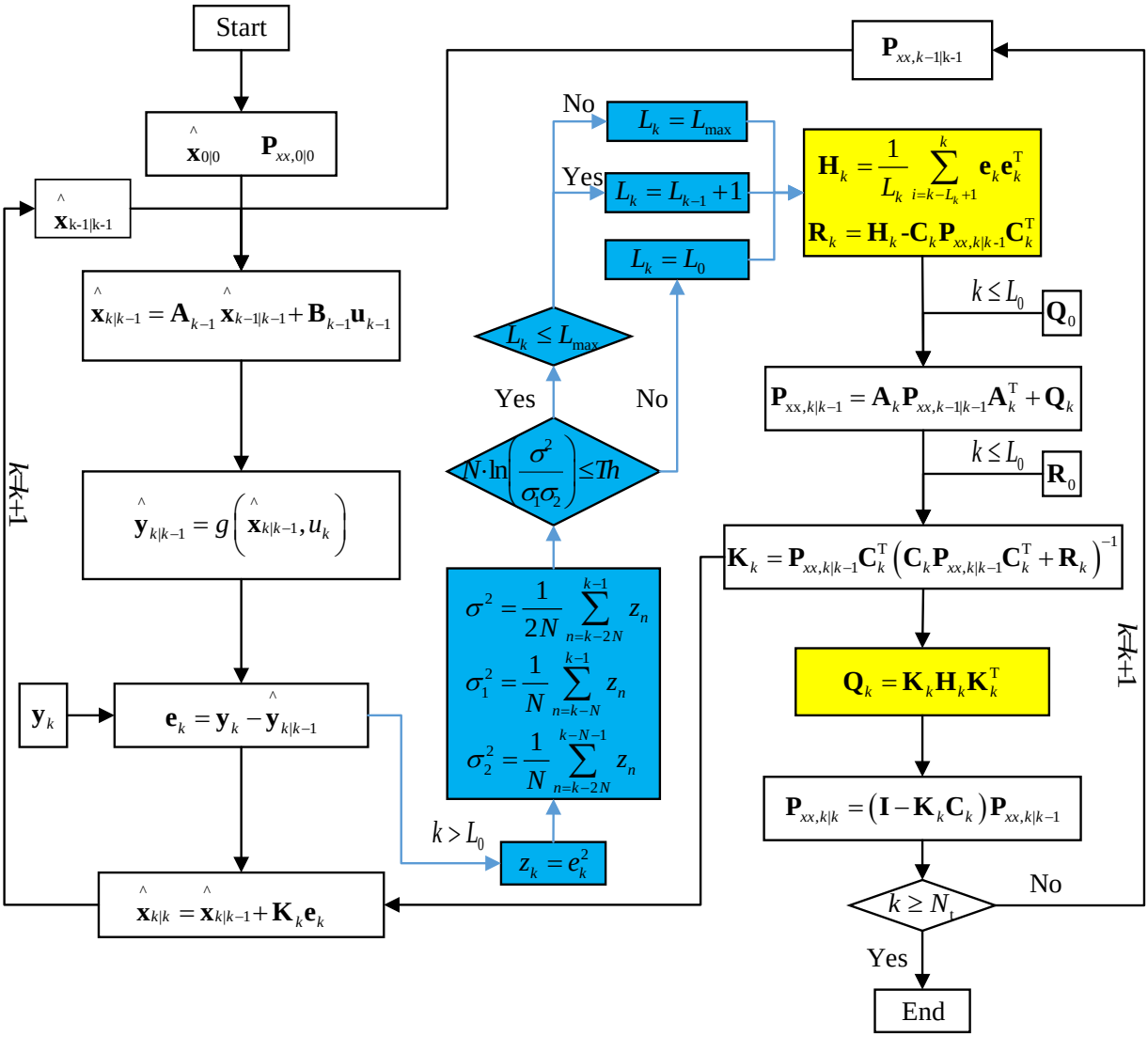

Fig. 2. Flow chart of IAEKF-based SOC estimation

5. Results and discussion

5.1 Parameter identification of the battery model

The random charge and discharge test data (RW9.mat) provided by NASA PCoE [63] is used to verify the proposed IAEKF method. The research object is the second generation 18650 LiCoO2 battery provided by Idaho National Laboratory. The nominal battery capacity is 2.1002Ah. The battery is tested at room temperature 25 ℃. For the random charge and discharge test, the batteries operate under a sequence of random generated charging and discharging currents between -4.5A and 4.5A. Each of loading periods last 5 minutes. The parameters $(K_0, K_1, \ldots, K_n)$ of the OCV model and the parameters (R_s, R_p, C_p) of ECM are first determined. A 12-degree polynomial function was found to be most suitable for fitting the OCV-SOC data. Fig. 3 shows the original data and fitting results, and Table 1 lists the corresponding parameters. The RMSE and MAE of the OCV estimation are 0.00337 V and 0.00264V, respectively, indicating that the proposed 12-degree polynomial OCV model has high accuracy. As the gradient of the OCV curve varies with SOC, the error of linear Taylor approximation caused by differentiating measurement equation $g(\mathbf{x}_k, \mathbf{u}_k)$ for $\mathbf{C}_k$ in the AEKF will also vary, which will influence the distribution of EIS in the AEKF-based SOC estimation.

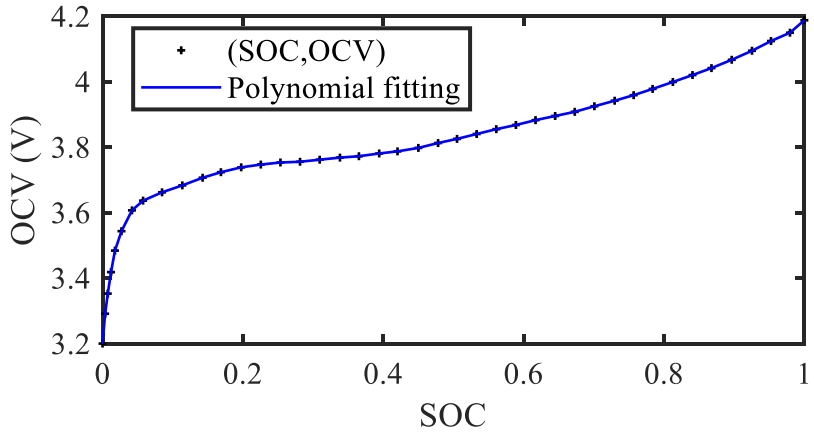

Fig. 3. OCV-SOC measurement points and polynomial fitting curve

Table 1. Parameters of OCV model

K_i	K_0	K_1	K_2	K_3	K_4	K_5
value	-3.884e+4	2.503e+5	-7.131e+5	1.183e+6	-1.266e-6	9.151e+5

K_6	K_7	K_8	K_9	K_{10}	K_{11}	K_{12}
-4.537e+5	1.540e+5	-3.497e+4	5.093e+3	-444.544	21.481	3.212

Based on the obtained OCV model, the initial parameters of the ECM can be estimated using genetic algorithm (GA). The pulse discharge current and the corresponding terminal voltage are shown in Fig. 4. Table 2 lists the initial parameters (R_s, R_p, C_p) of the ECM estimated based on the GA with the pulse discharge data.

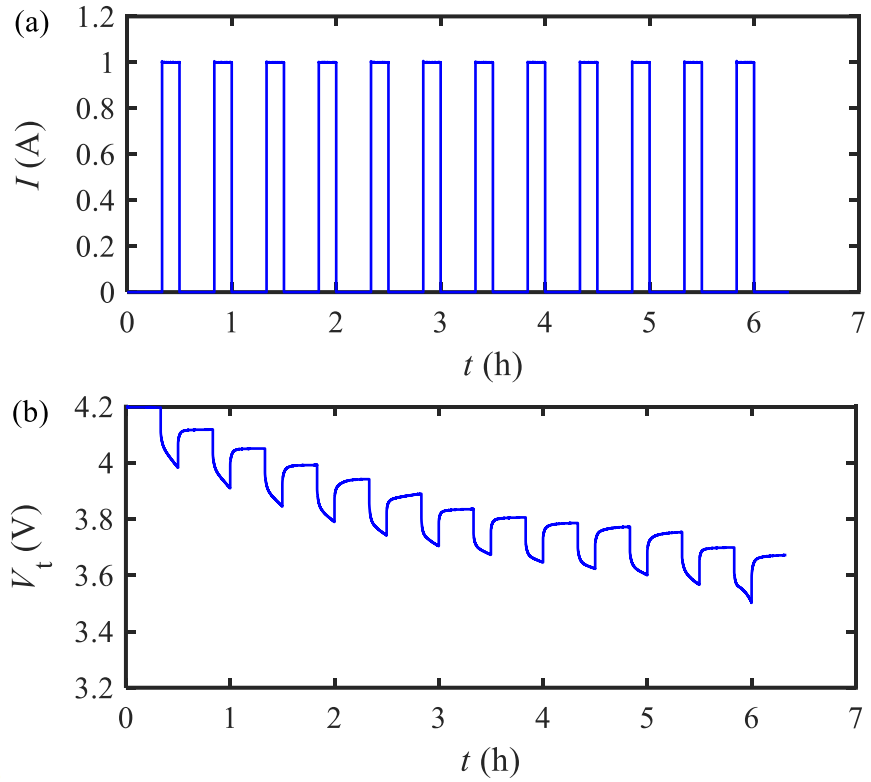

Fig. 4. (a) Pulse discharge current, and (b) terminal voltage

Table 2. Initial parameter values of ECM

Parameter	R_s	R_p	C_p
value	0.074	0.045	815

The test data can be downloaded from the official website of NASA, which is attached in the part of **Acknowledgement**. Considering that the test data collected covers a significant time due to

the relatively lengthy charge step, the terminal voltage and current within the 1st hour are used to verify the proposed IAEKF method. The terminal voltage and current under random charge and discharge are shown in Fig. 5.

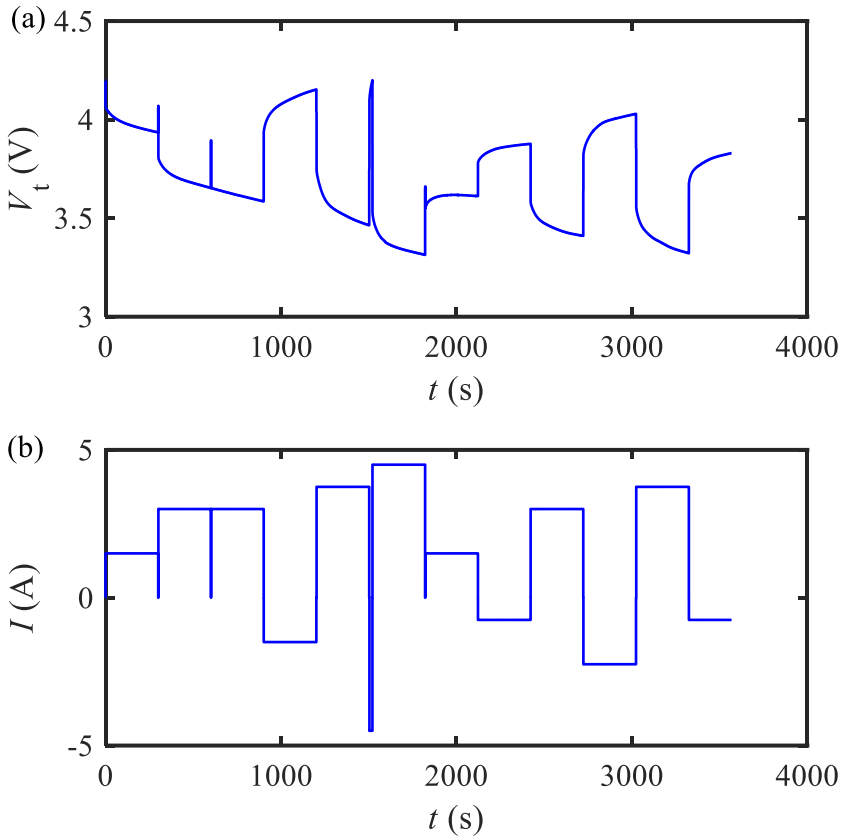

Fig. 5. (a) Battery terminal voltage V_t, and (b) current I under random discharge and charge test

As the parameters of the ECM change under the random discharge and charge condition, FF-RLS is used to estimate these parameters online. The parameter identification results of ECM are shown in Fig. 6.

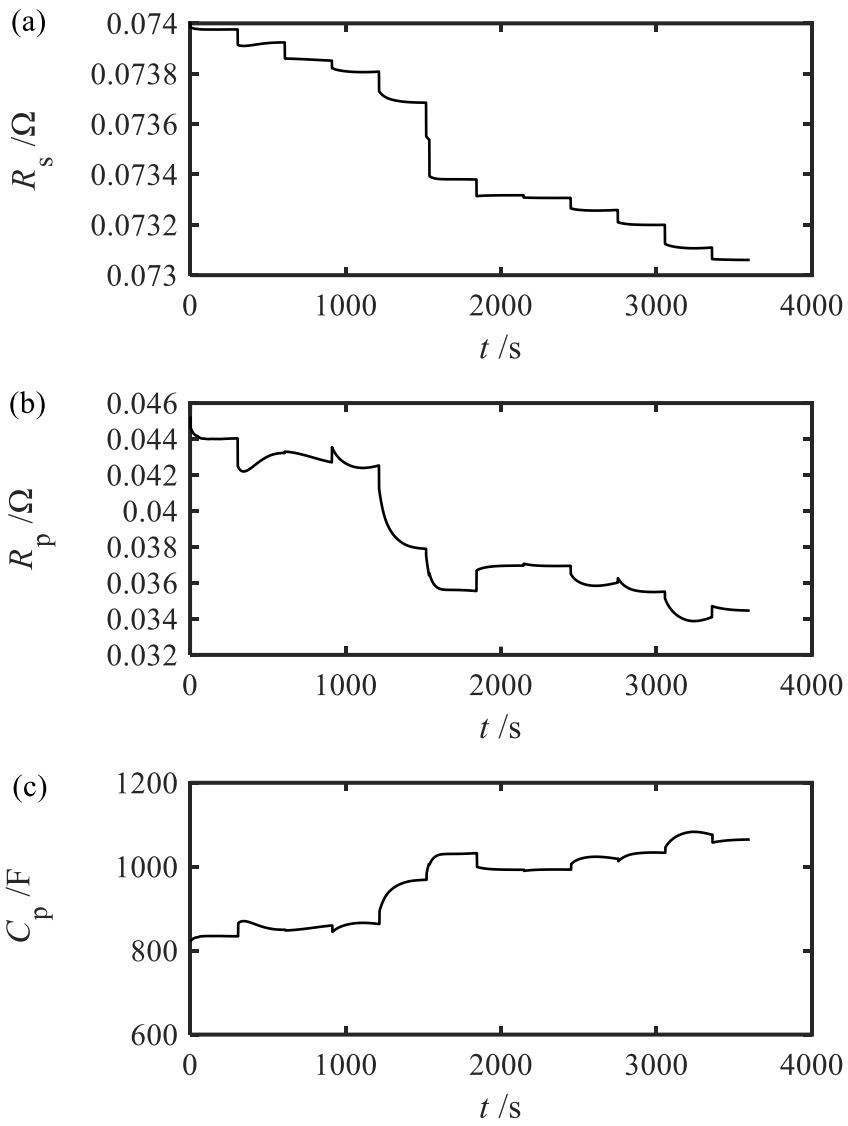

Fig. 6. Estimated parameter values of R_s, R_p and C_p

Fig. 7 shows the estimated terminal voltage and its error. The estimated voltage curve in blue is consistent with the measured terminal voltage, as shown in Fig. 7 (a). The RMSE and MAE of terminal voltage estimates are 0.00108 and 0.00063, respectively, which indicates the high accuracy of parameter identification of the ECM.

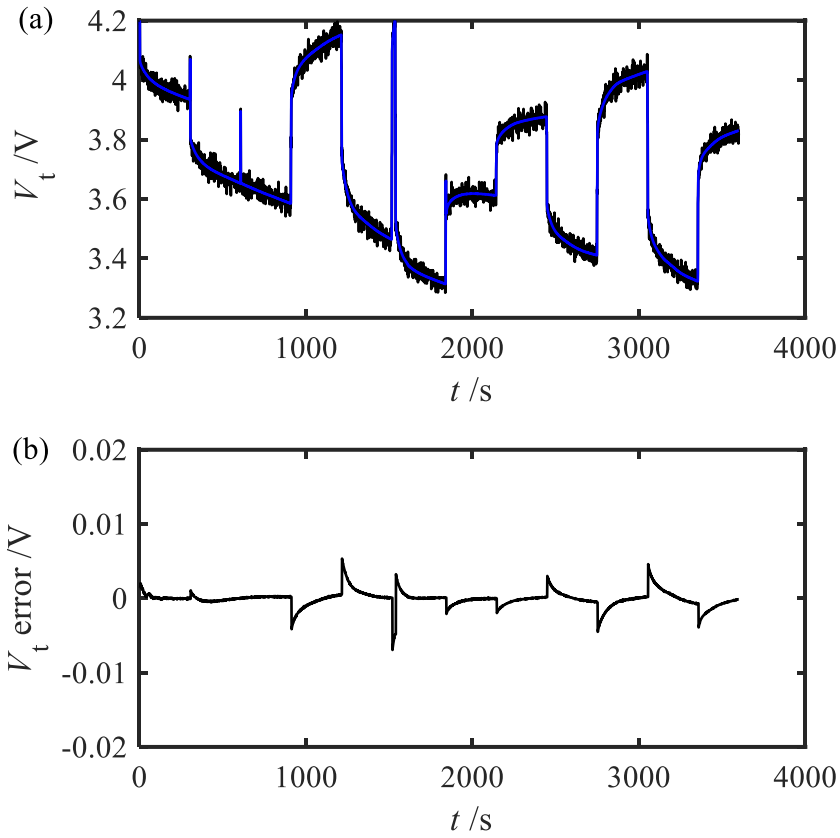

Fig. 7. (a) Estimated terminal voltage, and (b) its error based on the FF-RLS method

5.2 Verification of IAEKF-based SOC estimation

Initial parameters in the proposed IAEKF algorithm are needed for SOC estimation. Table 3 listed initial parameters [64] .

Table 3. Initial parameter values for SOC estimation

Parameters	value
Initial state $x_0=[V_{p,0}, SOC_0]^T$	$[0\ 0.9]^T$
Initial state error covariance matrix $\mathbf{P}_0$	[1e-3, 0; 0, 1e-2]
Process noise covariance matrix $\mathbf{Q}_0$	[1e-4, 0; 0, 1e-12]
Measurement noise covariance matrix R_0	5e-3

To verify the proposed IAEKF method, the EIS during the process of SOC estimation is given, as shown in Fig. 8. The EIS is affected by load current dynamics and error of the battery model. In addition, the EIS is also affected by the Taylor linear approximation of the AEKF method. As shown in Fig. 8, it is obvious that the EIS does not follow the Gaussian distribution with zero mean value for the whole duration. Therefore, the ICM should not be estimated with fixed length EIS, but rather the

moment of distribution change of the EIS should be detected, after which the subsequent EIS can be used to update ICM.

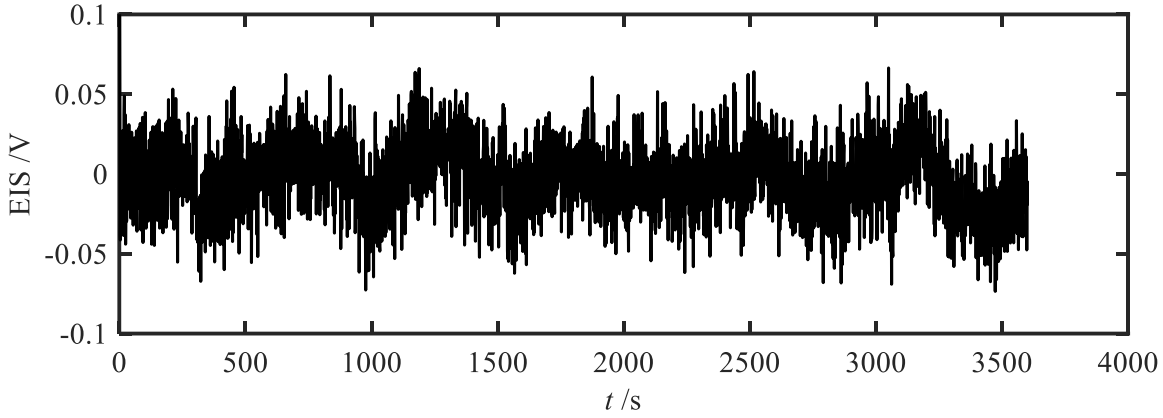

Fig. 8. Error innovation sequence

Based on the IAEKF method, the moment of distribution change of EIS is detected. According to the adaptive tuning rule described by Eq. (31), the length of the selected EIS gradually increases if $F_2 - F_1$ is less than the specified threshold, which means that the measurement noise does not change significantly. Once $F_2 - F_1$ exceeds the specified threshold, the window length of the selected EIS will set to 2 in order to adapt to the distribution change of EIS. In Fig. 9 (a), (b) and (c), the window length of the selected EIS constantly cycle from 2 to 4. In order to illustrate the adaptive tuning rule clearly, the partial enlarged drawing ranging from 1450 to 1500 is shown in Fig. 9 (d). If the distribution changes quickly, the length of the EIS may be reset to 2 once it reaches 3, which means $F_2 - F_1$ surpasses the specified threshold. If the distribution changes gradually, the window length of the selected EIS may increase gradually from 2 to 4 as $F_2 - F_1$ is less than the specified threshold Th. According to trying method, this threshold is set to 1. However, in order to reduce the online computation load, the maximum window length of the selected EIS must be set. Here, the maximum window length $L_{\max}$ is set to 4.

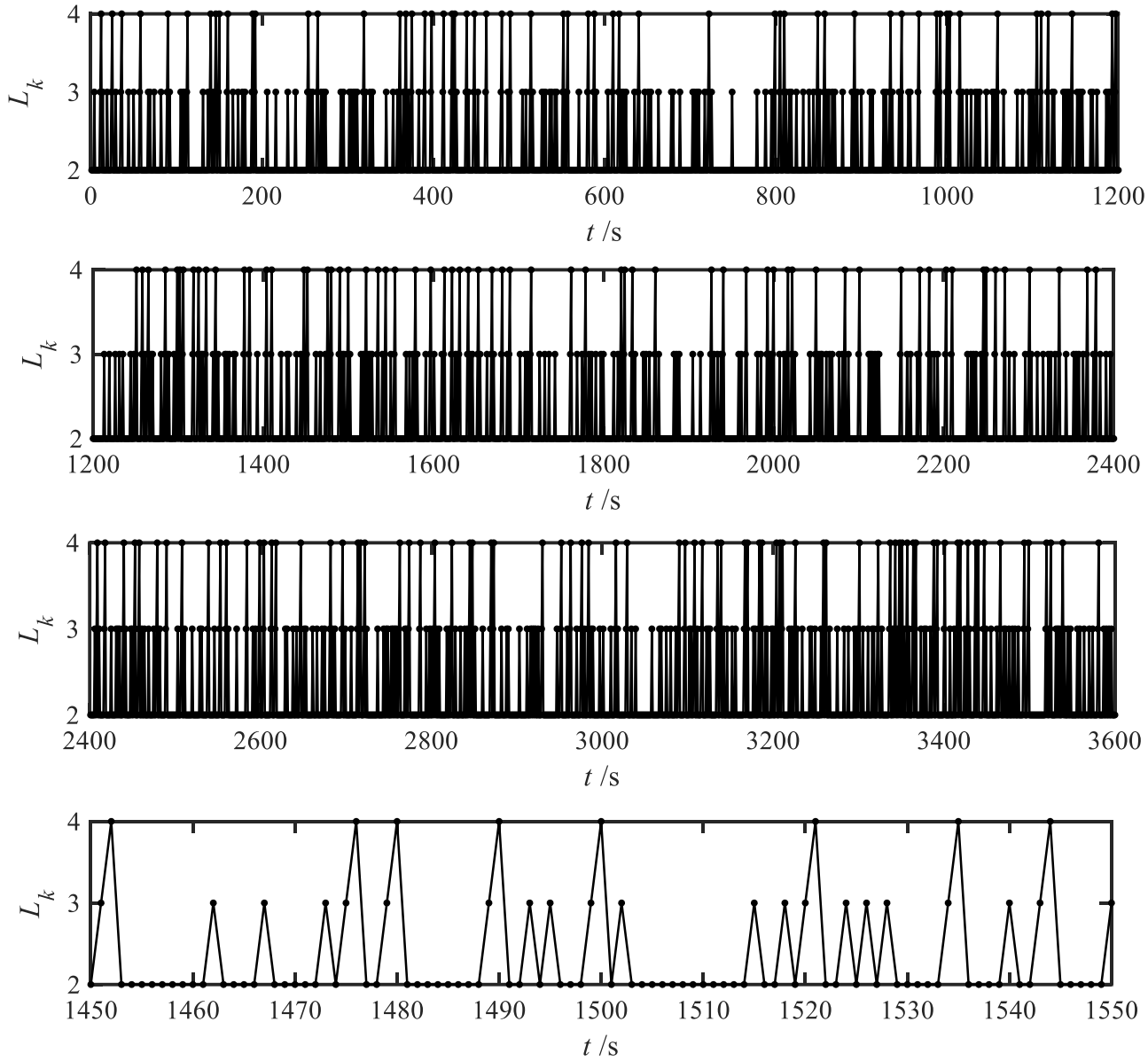

Fig. 9. (a), (b) and (c) Selected EIS length, and (d) local enlarged drawing

The selected EIS will be used to estimate the ICM, according to Eq. (35). Then the measurement and process noise are estimated based on Eq. (36) with the obtained ICM. Based on the proposed IAEKF method, the SOC estimation results are shown in Fig. 10. It shows that the SOC estimation results based on the IAEKF are very close to the reference SOC. The local enlarged drawing in Fig. 10 (a) shows that the SOC converges quickly to the reference SOC. Fig. 10 (b) shows that the

maximum SOC error of IAEKF method is around 0.01, and the SOC error quickly converges to zero over time.

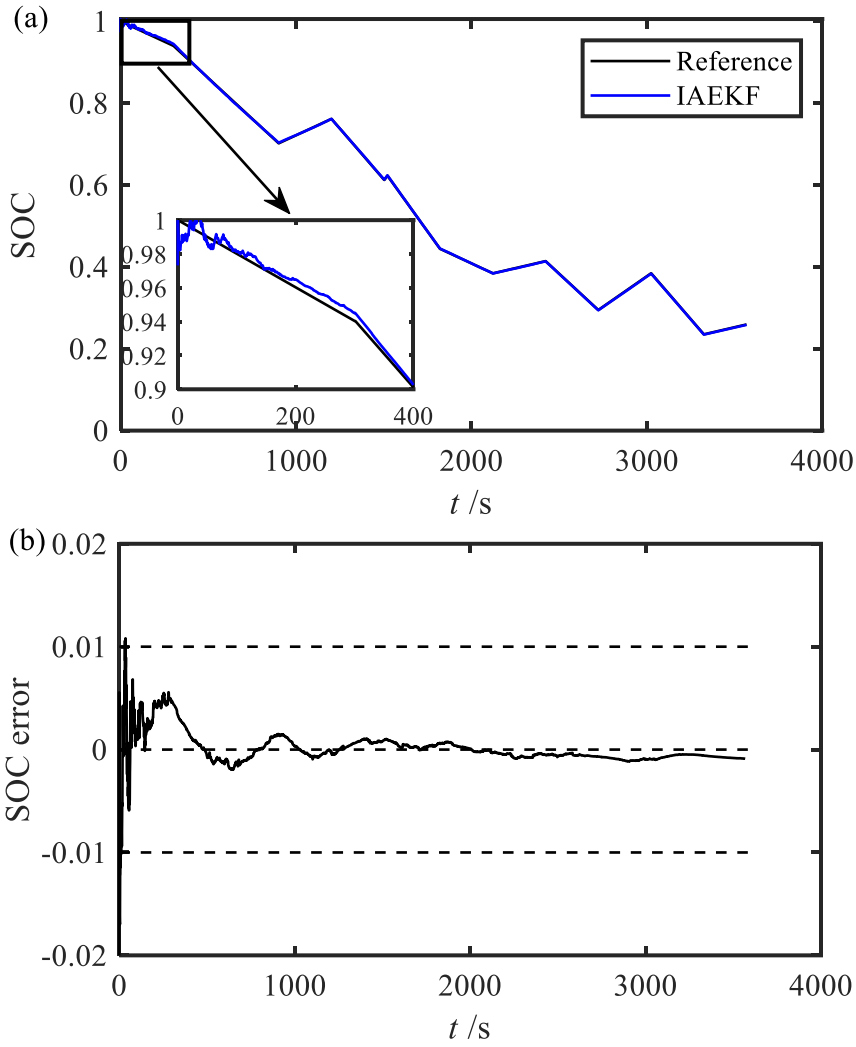

Fig. 10. (a) Estimated SOC, and (b) its error based on IAEKF

In order to demonstrate the superiority of the IAEKF method, the SOC results based on different methods are given, as shown in Fig. 11. The SOC obtained by coulomb counting method is usually adopted as reference SOC for comparison due to the test equipment has high accuracy. The local enlarged drawings in Fig. 11 (a) shows that the SOC result based on IAEKF is closer to the reference SOC than the one based on AEKF method. The parameters are initialized with the same parameters in Table 3. The fixed window length of AEKF method is 4. As shown in Fig. 11 (b), the maximum

SOC error based on IAEKF method is around 0.01, while the one based on AEKF method surpasses the 0.01 obviously. The fluctuation degree of SOC error based on the proposed IAEKF method is also smaller than the one based on AEKF method. Fig. 11 (b) shows that the SOC error decreases significantly in the time range [300s, 1000s] and [1200s, 2500s], which can be attributed to dynamic window length used to update ICM. For example, the maximum SOC error occurs around 1500s based on AEKF method, as shown in Fig. 11 (b). At this time, the resistance changes suddenly, as shown in Fig. 6 (a) and (b), due to the randomly generated large discharge current.

In the AEKF method, the ICM is estimated based on fixed window length EIS, which leads to a decrease of SOC accuracy. However, in the proposed IAEKF method, the length of EIS used to estimate the ICM is adaptive. As shown in Fig. 9 (d), the length of EIS is set to the small value 2 around 1500s, where the resistances change suddenly. As a result, the SOC accuracy is improved noticeably around 1500s, which demonstrates the superior performance of the proposed IAEKF method to the existing AEKF method.

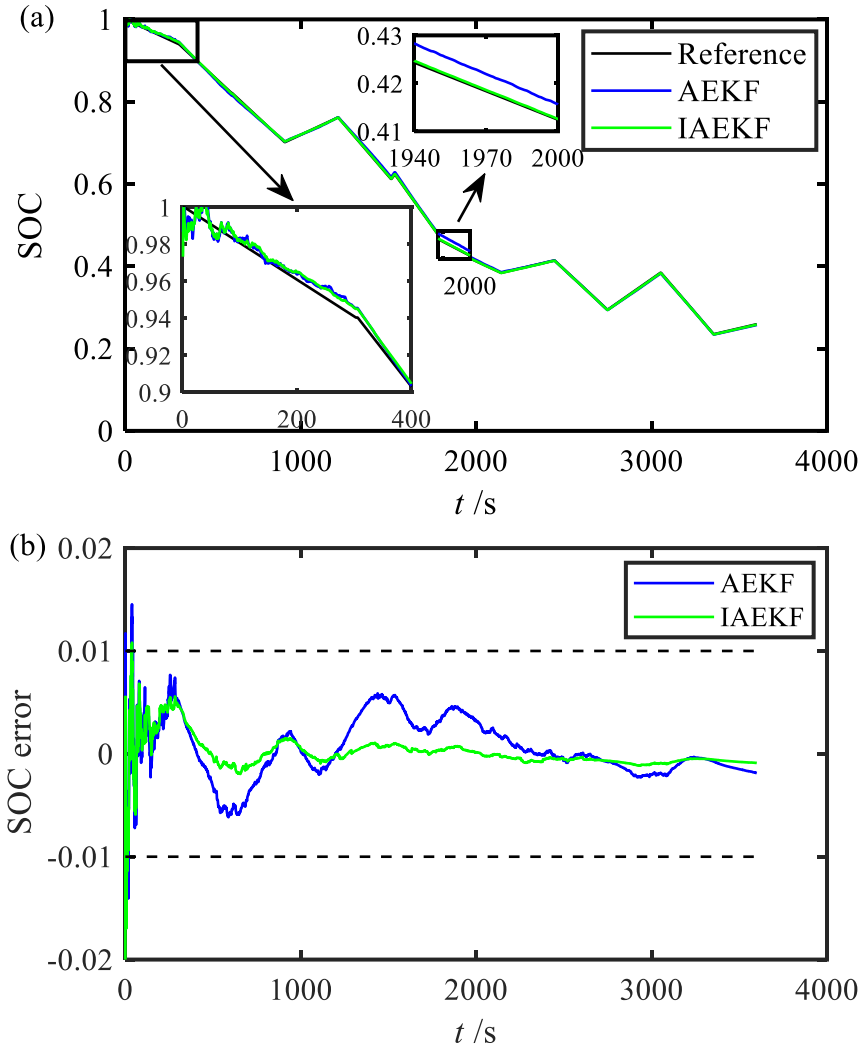

Fig. 11. (a) Estimated SOC, and (b) its error under different methods

To quantitatively compare the performance of these two methods, the corresponding RMSE and MAE of SOC are listed in Table 4. The proposed IAEKF has a higher accuracy than AEKF-based SOC estimation method. Compared with the RMSE and MAE of the AEKF method, the RMSE and MAE of the proposed IAEKF decrease by 43.34% and 55.80% respectively, which demonstrates the superiority of the proposed method.

Table 4. RMSE and MAE of SOC under different methods

Method	AEKF	IAEKF
RMSE	0.00293	0.00166
MAE	0.00224	0.00099

This computational time is the execution time of Matlab script on a PC with Intel Core(TM) i7-4710MQ processor and 8.0GB memory. As the execution process of Matlab scripts of AEKF and

IAEKF methods are affected by the states of the PC, such as CPU, memory and so on, the computation times of AEKF and IAEKF methods are random. In order to accurately evaluate the computation times of AEKF and IAEKF methods, the Matlab scripts of AEKF and IAEKF methods are executed 50 times respectively for statistical evaluation. As shown in Fig. 12, the average computation time of IAEKF method is slightly longer than that of AEKF method.

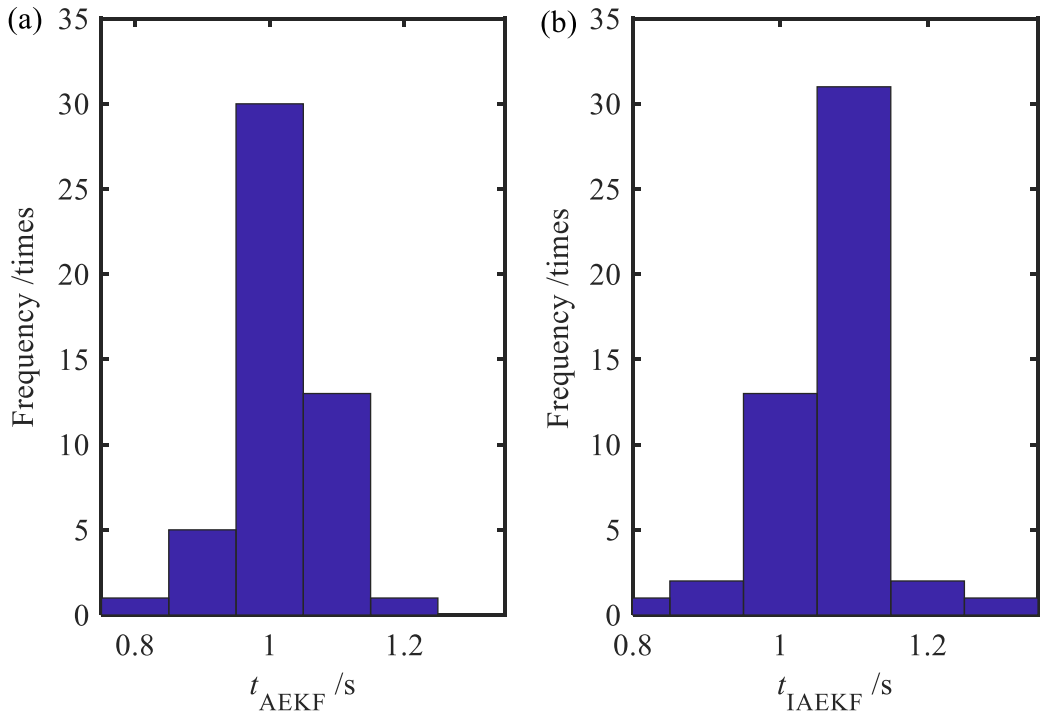

Fig. 12 Frequency histogram of computation time based on different methods

In order to quantitative evaluates the computation times of AEKF and IAEKF methods, the average and standard error of computation times of AEKF and IAEKF methods are listed in Table. 5. Compared with the computation time of AEKF method, the computation time of the proposed IAEKF increases by 4.59%. The SOC accuracy of IAEKF method is significantly improved at the cost of slightly increased computation time.

Table 5. Computation time under different methods

Method	AEKF	IAEKF
Average computation time (s)	1.0194	1.0662
Standard error of computation time (s)	0.0592	0.0733

5.3 Robustness analysis of the proposed IAEKF method

5.3.1 The effect of initial window length of EIS on SOC estimation

The SOC accuracy is affected by the ICM, which is estimated by selected EIS. Therefore, the initial window length of EIS will affect the SOC estimation accuracy. In order to evaluate the robustness of the proposed IAEKF method, the effect of the initial length of EIS on SOC estimation is evaluated, as shown in Fig. 13.

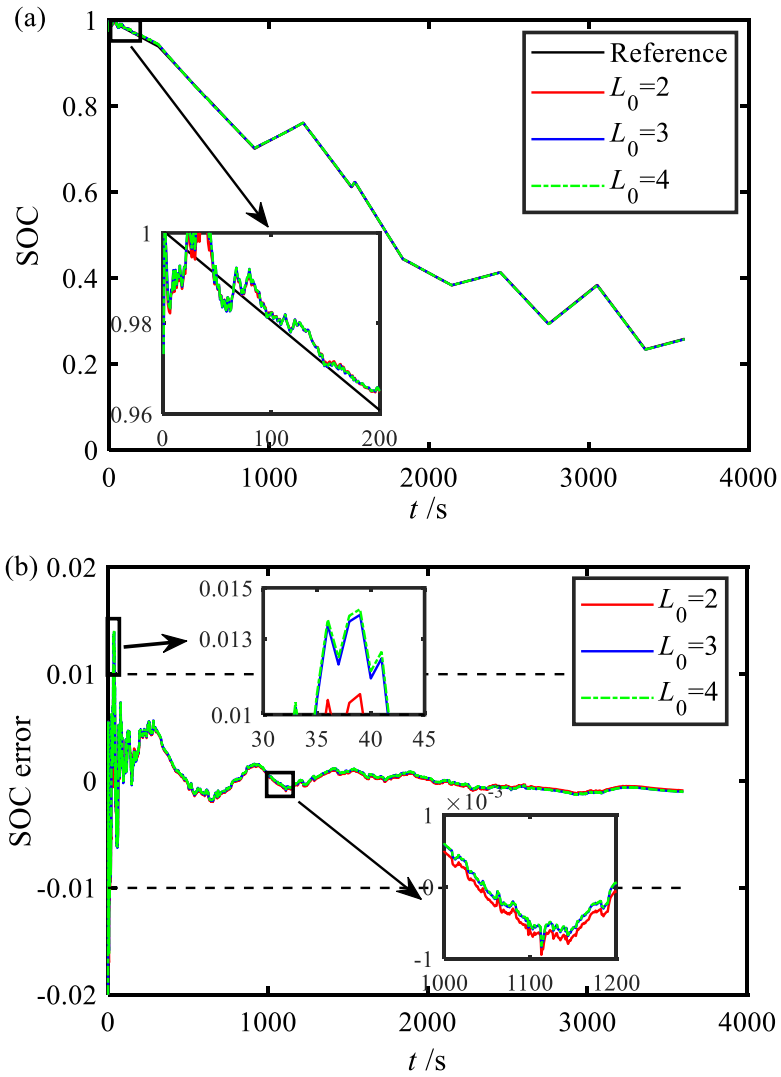

Fig. 13. Effect of L_0 on (a) SOC and (b) its error

As shown in Fig. 13 (a), the estimated SOC converges to the reference SOC quickly. The convergence process changes slightly with a different initial window length of EIS. The local

enlarged drawing in Fig. 13 (b) shows that the initial length of EIS L_0 affects the early convergence process of SOC.

To quantitatively evaluate the effect of the initial length of EIS on the SOC accuracy based on the IAEKF, the corresponding RMSE and MAE of SOC are listed in Table 6. It can be found that the RMSE of SOC increases significantly when L_0 increases from 2 to 3. Therefore, choosing proper initial length of EIS can improve the early convergence performance based on the IAEKF method. The MAE of SOC only increases by 7.07% when L_0 increases from 2 to 3. The reason is that the SOC error converges to the same value as time increases although the initial length of EIS is different. Therefore, the proposed IAEKF method is robust against initial length of EIS as time increases.

Table 6. RMSE and MAE under different initial length of EIS

Initial length of EIS	L_0=2	L_0 = 3	L_0=4
RMSE of SOC	0.00166	0.00174	0.00177
MAE of SOC	0.00099	0.00106	0.00107

5.3.2 The effect of initial measurement noise covariance value on SOC estimation

Initial measurement noise covariance is also an important parameter that affects the SOC estimation based on the IAEKF method. The effect of initial measurement noise covariance on the SOC estimation is also analysed, as shown in Fig. 14. Fig. 14 (a) indicates that the proposed IAEKF is robust to initial measurement noise covariance. The local enlarged drawing in Fig. 14 (a) shows that the estimated SOC under different initial measurement noise covariance is almost overlapped. Fig. 14 (b) shows that the SOC error tends to approach zero with the time although the initial measurement noise covariance is different. The local enlarged drawing in Fig. 14 (b) shows that the initial measurement noise has little effect on the convergence process of the IAEKF method.

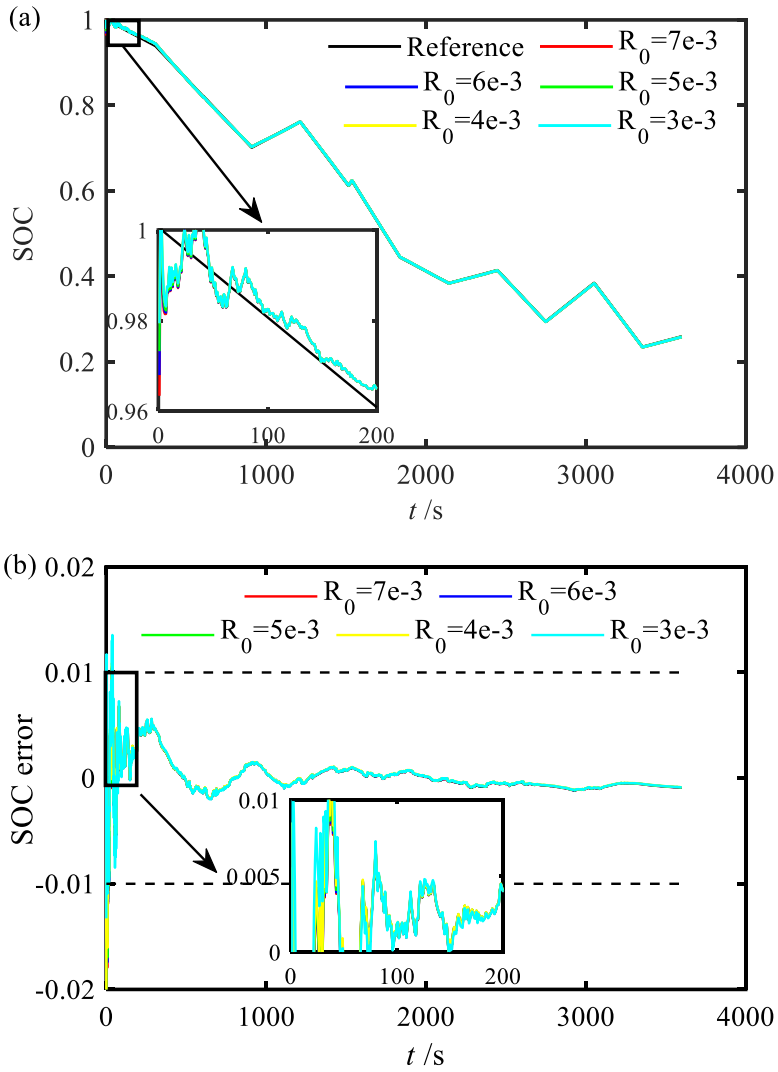

Fig. 14. The effect of R_0 on (a) SOC and (b) its error

In order to quantitatively evaluate of initial measurement noise value on the SOC based on the proposed IAEKF, the corresponding RMSE and MAE of SOC are listed in Table 7. It can be found that the RMSE and MAE of SOC have no obvious change, which indicates that the proposed IAEKF is resistant to initial measurement noise value.

Table 7. RMSE and MAE under different initial measurement noise covariance

IAEKF	R_0=7e-3	R_0=6e-3	R_0 = 5e-3	R_0=4e-3	R_0=3e-3
RMSE of SOC	0.00174	0.00170	0.00166	0.00162	0.00162
MAE of SOC	0.00100	0.00099	0.00099	0.00098	0.00099

In order to demonstrate the superiority of the proposed IAEKF method, RMSE and MAE under different initial SOC values based on AEKF method are listed in Table 8.

Table 8. RMSE and MAE under different initial measurement noise covariance

AEKF	R_0=7e-3	R_0=6e-3	R_0 = 5e-3	R_0=4e-3	R_0=3e-3
RMSE of SOC	0.00297	0.00295	0.00293	0.00291	0.00289
MAE of SOC	0.00225	0.00224	0.00224	0.00223	0.00222

In comparison of Table 7 and 8, the RMSE and MAE of SOC based on IAEKF method under different initial measurement noise covariance are significantly lower than the one based on AEKF method. The maximum RMSE and MAE of SOC based on IAEKF method are lower than the minimum one based on AEKF method. To sum up, the performance of the proposed method is better than the one of AEKF method.

5.3.3 Effect of initial SOC value on SOC estimation

Initial SOC value is an important factor that affects the SOC estimation based on the proposed IAEKF. As shown in Fig. 15 (a), the proposed IAEKF method is robust to the initial SOC value. Fig. 15 (b) indicates that the initial SOC significantly affects the early SOC error value, however the SOC error gradually converges to zero. The effect of initial SOC value on the SOC error decreases with time. In order to improve the SOC accuracy and convergence speed, the initial SOC should be set to the actual value as close as possible.

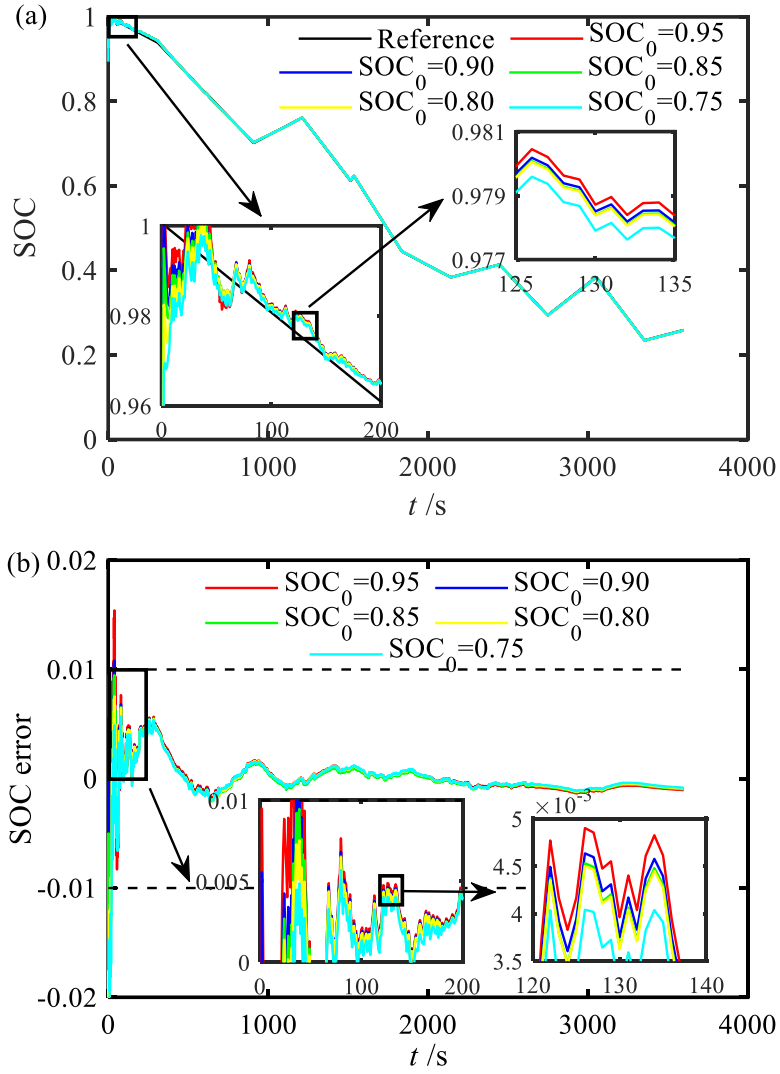

Fig. 15. The effect of SOC0 on (a) SOC and (b) its error

In order to quantitatively evaluate of initial SOC value on the SOC estimation based on the proposed IAEKF, the corresponding RMSE and MAE of SOC are listed in Table 9. It can be found that the RMSE of SOC increases as the initial SOC value deviates from the actual SOC value. This is mainly caused by the adaptive process of SOC. However, the MAE of SOC does not increase significantly as the initial SOC value deviates from the actual value. The reason is that the SOC error converges to zero with the time.

Table 9. RMSE and MAE under different initial SOC values

IAEKF	SOC_0=0.95	SOC_0 = 0.90	SOC_0=0.85	SOC_0=0.80	SOC_0=0.75
RMSE of SOC	0.00166	0.00171	0.00187	0.00220	0.00272

MAE of SOC	0.00099	0.00108	0.00102	0.00105	0.00104

To demonstrate the superiority of the proposed IAEKF method, RMSE and MAE under different initial SOC values based on AEKF method are listed in Table 10.

Table 10. RMSE and MAE under different initial SOC values

AEKF	SOC_0=0.95	SOC_0 = 0.90	SOC_0=0.85	SOC_0=0.80	SOC_0=0.75
RMSE of SOC	0.00290	0.00293	0.00307	0.00329	0.00367
MAE of SOC	0.00222	0.00224	0.00227	0.00231	0.00236

In comparison of Table 9 and 10, the RMSE and MAE of SOC based on IAEKF method under different initial SOC values are significantly lower than the one based on AEKF method. The maximum RMSE and MAE of SOC based on IAEKF method are lower than the minimum one based on AEKF method. In conclusion, the performance of the proposed method is better than the AEKF method.

6. Conclusions

AEKF has been widely used for battery SOC estimation based on ECM, and the accurate estimation of the ICM based on the EIS are key to the AEKF performance. To address the issue of the distribution change of EIS caused by load current dynamics, error of battery model and linear Taylor approximation of AEKF, an IAEKF method is proposed as a way of improving the SOC estimation accuracy of LIBs. The following are conclusions drawn from this work:

(1) Compared to AEKF, IAEKF leads to 43.34% and 55.80% improvement in the estimation accuracy of RMSE and MAE of SOC, respectively. The maximum SOC error based on the proposed IAEKF method is around 0.01 when the initial window length used for EIS covariance estimation is set to 2, which is significantly lower than the one based on AEKF method.

(2) With the significant improvement of RMSE and MAE, the computation time of the proposed IAEKF method increases by only 4.59%, thus it can be used for online estimation.

(3) The effect of the initial length of EIS on SOC results based on IAEKF method is analysed. The initial length of EIS affects the early convergence process of SOC. Selecting proper initial length of EIS can improve the early convergence performance of SOC. The SOC error converges to almost the same value as time increases. Therefore, the proposed IAEKF method is robust against the initial length of EIS.

(4) The effect of initial measurement noise covariance on SOC results based on IAEKF method is analysed. The RMSE and MAE of SOC have no obvious change, which indicates that the proposed IAEKF is robust to initial measurement noise value. The compared results indicate that the performance of the proposed IAEKF method is significantly better than AEKF based method.

(5) The influence of initial SOC value on SOC results based on IAEKF method is analysed. The maximum RMSE and MAE of SOC based on IAEKF method are smaller than the one based on the AEKF method, which demonstrates the superiority of the performance of the proposed IAEKF method.

In the short term, the influence of ageing on SOC estimation of lithium-ion battery is not significant, however, in the long term such influence can't be ignored. As the battery ages, the capacity of LIBs will change, which would also contribute to the distribution change of EIS in the AEKF method. In this case, this algorithm proposed in this paper has the potential to enable more accurate online SOC estimation, which would constitute future work.

Acknowledgements

The authors would like to thank the data provided by NASA Ames Prognostics Center from https://ti.arc.nasa.gov/tech/dash/groups/pcoe/prognostic-data-repository/. The work has received support from the UK-China Joint Research and Innovation Partnership fund from China Scholarship Council (CSC) and British Council (BC) under the grant number 201703780098 and the grants from

the National Natural Science Foundation of China under grant number No. 51806189 and No. 51476143. The authors also would like to thank the supports from NSFC-RS Joint Project under the grant number No. 5151101443 and IE/151256. The support from Cao Guang Biao High Tech Talent Fund, Zhejiang University is also highly acknowledged. This work also received support from EPSRC for project TRENDS (reference number EP/R020973/1).

References

[1] Zheng L, Zhu J, Lu DD-C, Wang G, He T. Incremental capacity analysis and differential voltage analysis based state of charge and capacity estimation for lithium-ion batteries. Energy. 2018;150:759-69.
[2] Sun L, Li G, You F. Combined internal resistance and state-of-charge estimation of lithium-ion battery based on extended state observer. Renewable and Sustainable Energy Reviews. 2020;131:109994.
[3] Yang Y, Bremner S, Menictas C, Kay M. Battery energy storage system size determination in renewable energy systems: A review. Renewable and Sustainable Energy Reviews. 2018;91:109-25.
[4] Peng J, Luo J, He H, Lu B. An improved state of charge estimation method based on cubature Kalman filter for lithium-ion batteries. Applied Energy. 2019;253.
[5] Pastor-Fernández C, Yu TF, Widanage WD, Marco J. Critical review of non-invasive diagnosis techniques for quantification of degradation modes in lithium-ion batteries. Renewable and Sustainable Energy Reviews. 2019;109:138-59.
[6] Xia B, Chen C, Tian Y, Wang M, Sun W, Xu Z. State of charge estimation of lithium-ion batteries based on an improved parameter identification method. Energy. 2015;90:1426-34.
[7] Ng KS, Moo C-S, Chen Y-P, Hsieh Y-C. Enhanced coulomb counting method for estimating state-of-charge and state-of-health of lithium-ion batteries. Applied Energy. 2009;86:1506-11.
[8] Yang N, Zhang X, Li G. State of charge estimation for pulse discharge of a LiFePO4 battery by a revised Ah counting. Electrochimica Acta. 2015;151:63-71.
[9] Yang R, Xiong R, He H, Mu H, Wang C. A novel method on estimating the degradation and state of charge of lithium-ion batteries used for electrical vehicles. Applied Energy. 2017;207:336-45.
[10] Xing Y, He W, Pecht M, Tsui KL. State of charge estimation of lithium-ion batteries using the open-circuit voltage at various ambient temperatures. Applied Energy. 2014;113:106-15.
[11] Yang F, Li W, Li C, Miao Q. State-of-charge estimation of lithium-ion batteries based on gated recurrent neural network. Energy. 2019;175:66-75.
[12] Tang X, Gao F, Zou C, Yao K, Hu W, Wik T. Load-responsive model switching estimation for state of charge of lithium-ion batteries. Applied Energy. 2019;238:423-34.
[13] Li Y, Wang C, Gong J. A multi-model probability SOC fusion estimation approach using an improved adaptive unscented Kalman filter technique. Energy. 2017;141:1402-15.
[14] Shen Y. Improved chaos genetic algorithm based state of charge determination for lithium batteries in electric vehicles. Energy. 2018;152:576-85.
[15] Zheng F, Xing Y, Jiang J, Sun B, Kim J, Pecht M. Influence of different open circuit voltage tests on state of charge online estimation for lithium-ion batteries. Applied Energy. 2016;183:513-25.
[16] Yang F, Zhang S, Li W, Miao Q. State-of-charge estimation of lithium-ion batteries using LSTM and UKF. Energy. 2020;201:117664.
[17] Sheng H, Xiao J. Electric vehicle state of charge estimation: Nonlinear correlation and fuzzy support vector machine. Journal of Power Sources. 2015;281:131-7.
[18] Zahid T, Xu K, Li W, Li C, Li H. State of charge estimation for electric vehicle power battery using advanced machine learning algorithm under diversified drive cycles. Energy. 2018;162:871-82.
[19] Dai H, Guo P, Wei X, Sun Z, Wang J. ANFIS (adaptive neuro-fuzzy inference system) based online SOC (State of Charge) correction considering cell divergence for the EV (electric vehicle) traction batteries. Energy. 2015;80:350-60.

[20] He W, Williard N, Chen C, Pecht M. State of charge estimation for Li-ion batteries using neural network modeling and unscented Kalman filter-based error cancellation. International Journal of Electrical Power & Energy Systems. 2014;62:783-91.
[21] Chemali E, Kollmeyer PJ, Preindl M, Emadi A. State-of-charge estimation of Li-ion batteries using deep neural networks: A machine learning approach. Journal of Power Sources. 2018;400:242-55.
[22] Chemali E, Kollmeyer PJ, Preindl M, Ahmed R, Emadi A. Long Short-Term Memory Networks for Accurate State-of-Charge Estimation of Li-ion Batteries. IEEE Transactions on Industrial Electronics. 2018;65:6730-9.
[23] Tian Y, Lai R, Li X, Xiang L, Tian J. A combined method for state-of-charge estimation for lithium-ion batteries using a long short-term memory network and an adaptive cubature Kalman filter. Applied Energy. 2020;265:114789.
[24] Bian C, He H, Yang S. Stacked bidirectional long short-term memory networks for state-of-charge estimation of lithium-ion batteries. Energy. 2020;191:116538.
[25] Tang X, Liu B, Lv Z, Gao F. Observer based battery SOC estimation: Using multi-gain-switching approach. Applied Energy. 2017;204:1275-83.
[26] Zhang W, Wang L, Wang L, Liao C. An improved adaptive estimator for state-of-charge estimation of lithium-ion batteries. Journal of Power Sources. 2018;402:422-33.
[27] Xu J, Mi CC, Cao B, Deng J, Chen Z, Li S. The State of Charge Estimation of Lithium-Ion Batteries Based on a Proportional-Integral Observer. IEEE Transactions on Vehicular Technology. 2014;63:1614-21.
[28] Xiong R, Yu Q, Wang LY, Lin C. A novel method to obtain the open circuit voltage for the state of charge of lithium ion batteries in electric vehicles by using H infinity filter. Applied Energy. 2017;207:346-53.
[29] Liu C, Zhu Q, Li L, Liu W, Wang L, Xiong N, et al. A State of Charge Estimation Method Based on H_∞ Observer for Switched Systems of Lithium-Ion Nickel–Manganese–Cobalt Batteries. IEEE Transactions on Industrial Electronics. 2017;64:8128-37.
[30] Li W, Liang L, Liu W, Wu X. State of Charge Estimation of Lithium-Ion Batteries Using a Discrete-Time Nonlinear Observer. IEEE Transactions on Industrial Electronics. 2017;64:8557-65.
[31] Tian Y, Li D, Tian J, Xia B. State of charge estimation of lithium-ion batteries using an optimal adaptive gain nonlinear observer. Electrochimica Acta. 2017;225:225-34.
[32] Zou Y, Hu X, Ma H, Li SE. Combined State of Charge and State of Health estimation over lithium-ion battery cell cycle lifespan for electric vehicles. Journal of Power Sources. 2015;273:793-803.
[33] Deng Z, Yang L, Cai Y, Deng H, Sun L. Online available capacity prediction and state of charge estimation based on advanced data-driven algorithms for lithium iron phosphate battery. Energy. 2016;112:469-80.
[34] Wang S-L, Fernandez C, Zou C-Y, Yu C-M, Chen L, Zhang L. A comprehensive working state monitoring method for power battery packs considering state of balance and aging correction. Energy. 2019;171:444-55.
[35] Tanim TR, Rahn CD, Wang C-Y. State of charge estimation of a lithium ion cell based on a temperature dependent and electrolyte enhanced single particle model. Energy. 2015;80:731-9.
[36] Deng Z, Yang L, Deng H, Cai Y, Li D. Polynomial approximation pseudo-two-dimensional battery model for online application in embedded battery management system. Energy. 2018;142:838-50.
[37] Nejad S, Gladwin DT, Stone DA. A systematic review of lumped-parameter equivalent circuit models for real-time estimation of lithium-ion battery states. Journal of Power Sources. 2016;316:183-96.
[38] Lai X, Zheng Y, Sun T. A comparative study of different equivalent circuit models for estimating state-of-charge of lithium-ion batteries. Electrochimica Acta. 2018;259:566-77.
[39] Weng C, Sun J, Peng H. A unified open-circuit-voltage model of lithium-ion batteries for state-of-charge estimation and state-of-health monitoring. Journal of Power Sources. 2014;258:228-37.
[40] Zhu Q, Xu M, Liu W, Zheng M. A state of charge estimation method for lithium-ion batteries based on fractional order adaptive extended kalman filter. Energy. 2019;187:115880.
[41] Shen P, Ouyang M, Lu L, Li J, Feng X. The Co-estimation of State of Charge, State of Health, and State of Function for Lithium-Ion Batteries in Electric Vehicles. IEEE Transactions on Vehicular Technology. 2018;67:92-103.
[42] Zheng Y, Gao W, Ouyang M, Lu L, Zhou L, Han X. State-of-charge inconsistency estimation of lithium-ion battery pack using mean-difference model and extended Kalman filter. Journal of Power Sources. 2018;383:50-8.
[43] Shen Y. Adaptive extended Kalman filter based state of charge determination for lithium-ion batteries. Electrochimica Acta. 2018;283:1432-40.
[44] Xiong R, Sun F, He H, Nguyen TD. A data-driven adaptive state of charge and power capability joint estimator of lithium-ion polymer battery used in electric vehicles. Energy. 2013;63:295-308.
[45] Li Y, Wang C, Gong J. A combination Kalman filter approach for State of Charge estimation of lithium-ion battery considering model uncertainty. Energy. 2016;109:933-46.
[46] Wang Y, Zhang C, Chen Z. A method for state-of-charge estimation of Li-ion batteries based on multi-model switching strategy. Applied Energy. 2015;137:427-34.

[47] Pan H, Lü Z, Lin W, Li J, Chen L. State of charge estimation of lithium-ion batteries using a grey extended Kalman filter and a novel open-circuit voltage model. Energy. 2017;138:764-75.
[48] He H, Xiong R, Peng J. Real-time estimation of battery state-of-charge with unscented Kalman filter and RTOS μCOS-II platform. Applied Energy. 2016;162:1410-8.
[49] Peng J, Luo J, He H, Lu B. An improved state of charge estimation method based on cubature Kalman filter for lithium-ion batteries. Applied Energy. 2019;253:113520.
[50] Chen Z, Sun H, Dong G, Wei J, Wu J. Particle filter-based state-of-charge estimation and remaining-dischargeable-time prediction method for lithium-ion batteries. Journal of Power Sources. 2019;414:158-66.
[51] Li X, Wang Z, Zhang L. Co-estimation of capacity and state-of-charge for lithium-ion batteries in electric vehicles. Energy. 2019;174:33-44.
[52] Peng S, Zhu X, Xing Y, Shi H, Cai X, Pecht M. An adaptive state of charge estimation approach for lithium-ion series-connected battery system. Journal of Power Sources. 2018;392:48-59.
[53] Li W, Fan Y, Ringbeck F, Jöst D, Han X, Ouyang M, et al. Electrochemical model-based state estimation for lithium-ion batteries with adaptive unscented Kalman filter. Journal of Power Sources. 2020;476:228534.
[54] Liu Z, Dang X, Jing B, Ji J. A novel model-based state of charge estimation for lithium-ion battery using adaptive robust iterative cubature Kalman filter. Electric Power Systems Research. 2019;177:105951.
[55] Linghu J, Kang L, Liu M, Luo X, Feng Y, Lu C. Estimation for state-of-charge of lithium-ion battery based on an adaptive high-degree cubature Kalman filter. Energy. 2019;189:116204.
[56] Ye M, Guo H, Cao B. A model-based adaptive state of charge estimator for a lithium-ion battery using an improved adaptive particle filter. Applied Energy. 2017;190:740-8.
[57] Wang L, Lu D, Liu Q, Liu L, Zhao X. State of charge estimation for LiFePO4 battery via dual extended kalman filter and charging voltage curve. Electrochimica Acta. 2019;296:1009-17.
[58] Wang Q, Kang J, Tan Z, Luo M. An online method to simultaneously identify the parameters and estimate states for lithium ion batteries. Electrochimica Acta. 2018;289:376-88.
[59] Guo F, Hu G, Xiang S, Zhou P, Hong R, Xiong N. A multi-scale parameter adaptive method for state of charge and parameter estimation of lithium-ion batteries using dual Kalman filters. Energy. 2019;178:79-88.
[60] Jiang B, Dai H, Wei X, Xu T. Joint estimation of lithium-ion battery state of charge and capacity within an adaptive variable multi-timescale framework considering current measurement offset. Applied Energy. 2019;253.
[61] Ye M, Guo H, Xiong R, Yu Q. A double-scale and adaptive particle filter-based online parameter and state of charge estimation method for lithium-ion batteries. Energy. 2018;144:789-99.
[62] Sun F, Xiong R. A novel dual-scale cell state-of-charge estimation approach for series-connected battery pack used in electric vehicles. Journal of Power Sources. 2015;274:582-94.
[63] Bole BK, C.S.; Daigle, M. Adaptation of an Electrochemistry-based Li-Ion Battery Model to Account for Deterioration Observed Under Randomized Use. In Proceedings of the Annual Conference of the Prognostics and Health Management Society. Fort Worth, TX, USA2014.
[64] Andersson J. Lifetime estimation of Lithium-ion batteries for stationary energy storage systems. Stockholm: KTH Royal Institute of Technology; 2017.